Supporting Information

for

P-doped PtNi alloy supported on N,C-doped TiO_2 nanosheets as stable electrocatalyst for oxygen reduction reaction in acidic electrolyte

*Chen Lu, Chao Xu, Peng-Peng Guo, Kun-Zu Yang, Ying Xu, Hua-Min Chi, Ping-Jie Wei and Jin-Gang Liu**

Key Lab for Advanced Materials, School of Chemistry & Molecular Engineering, East China University of Science and Technology, Shanghai, 200237, P. R. China. E-mail: liujingang@ecust.edu.cn

Materials and synthesis

Synthesis of N, C-doped TiO_2 nanosheets

The TiO_2 nanosheets were prepared using a hydrothermal method according to previous report.[1] Afterward, a mixture of the prepared TiO_2 nanosheets and urea with mass ratio of 1:5 was calcinated at 450 °C in high purity N_2 for 2 h, and naturally cooling to RT produced the N, C-doped TiO_2 nanosheets.

Synthesis of PtNi@N,C-TiO_2nanosheets

The obtained N,C-doped TiO_2 nanosheets (50 mg) were added into ethylene glycol (EG, 70 mL), and the resultant solution was ultrasonicated and stirred to form uniform slurry. Afterward, the Pt precursor $H_2PtCl_6 \cdot 6H_2O$ (84 mg) and the Ni precursor $NiCl_2 \cdot 6H_2O$ (40 mg) were added into the above uniform slurry, of which pH was adjusted to about 9-10 using 3.0 M NaOH solution. The slurry solution was stirred under heat at 150 °C in an oil bath for 5 h. After cooling to RT, the obtained slurry was separated by high-speed centrifugation, washed with distilled water and ethanol several times, and finally dried at 60 °C for 12 h to provide the PtNi@N,C-TiO_2 nanosheets.

Synthesis of P-doped PtNi on N,C-doped TiO_2 nanosheets (P-PtNi@N,C-TiO_2)

The obtained PtNi@N,C-TiO_2 nanosheets and NaH_2PO_2 with a mass ratio of 1:4 was separately

placed on a porcelain boat, which to be put in a tube furnace and was heated to 350 °C with rate of 5 °C min^{-1} under N_2 atmosphere and held on for 2 h, then naturally cooled to RT to produce the P-doped product P-PtNi@N,C-TiO_2 nanosheets.

Synthesis of P-doped PtNi on carbon black (P-PtNi@C)

The preparation process of P-doped PtNi@C was similar to that of P-PtNi@N,C-TiO_2 nanosheets, except that N,C-TiO_2 nanosheets were replaced by carbon black.

Materials Characterization

The morphology and structure of the prepared nanomaterials were investigated by transmission electron microscopy (TEM; JEM-1400) and high-angle annular dark-field scanning transmission electron microscopy (HAADF-STEM; Talos F200X). X-ray diffraction (XRD) spectra were recorded using the D/max2550VB/PC18KW, where the range of 2θ was 10-80°. XPS profiles were recorded on a Thermo Escalab 250 instrument with a monochromatic Al Kα X-ray source (hν =1486.6 eV). All binding energies were referenced to the C1s peak (284.6 eV) corresponding to adventitious carbon. Quantitative analysis of elements was performed using inductively coupled plasma-optical emission spectrometer (ICP-OES).

Electrochemical Measurements

Electrochemical performance of all catalysts was evaluated using a rotating ring-disk electrode (RRDE) on CHI 760D electrochemical work station via traditional three-electrode system. During the RRDE tests, the glassy carbon electrode was used as work electrode (diameter: 5 mm; geometric area: 0.196 cm^2), carbon rod as the counter electrode and Ag/AgCl as the reference electrode, respectively.

Catalyst ink preparation: The prepared catalyst (5.0 mg) was added to a glass vial with 25 μL of a 5 wt% Nafion (Aldrich) solution and 225 μL of isopropanol, which was subjected to sonication in a sonicator bath for 1 h to afford a homogeneous suspension. The loading amount of Pt with samples of P-PtNi@N,C-TiO_2, PtNi@N,C-TiO_2 and 20 wt% Pt/C (Vulcan XC-72, JM HiSPEC 3000) was 22, 18, and 100 μg cm^{-2}, respectively. Cyclic voltammetry (CV) and Linear sweep voltammetry (LSV) were conducted in an Ar or O_2-saturated 0.1 M $HClO_4$ solution at a scanning rate of 10 mV s^{-1} at room temperature. All potentials in this study were relative to the reversible hydrogen electrode (RHE).

The potential with respect to RHE can be calculated as follows:

$$E_{(RHE)} = E_{(Ag/AgCl)} + 0.059 \times pH + E^{\theta}_{(Ag/AgCl)}.$$

The Koutecky-Levich (K-L) equation was used to calculate the kinetic current density (j_K) of the catalysts at 0.9 V (vs. RHE) for the ORR kinetic process, which in turn led to the calculation of mass activity (MA) and specific activity (SA) [2].

$$\frac{1}{j} = \frac{1}{j_L} + \frac{1}{j_K}$$

where j was the measured current density and j_L was the limiting diffusion current density.

$$MA = \frac{j_K}{m_{Pt}}$$

Where m_{Pt} was the Pt loading of the catalysts used in the working electrode.

$$SA = \frac{MA}{ECSA}$$

Where *ECSA* was the electrochemical surface area of the catalyst, which could be estimated by H_{upd} method.

In addition, the ECSA was evaluated through hydrogen underpotential deposition (H_{upd}) (assumption factor = 210 μC cm^{-2}), which was performed in O_2-saturated 0.1 M $HClO_4$ with a sweep rate of 50 mV/s.[3] The ECSA was obtained via the H_{upd} method by the following equation.

$$ECSA = \frac{S_H / V}{0.21(mC\ \ cm^{-2}) * M_{Pt}}$$

S_H was the active specific surface area calculated from H adsorption/desorption, V represented the scan rate and M_{Pt} indicated the mass of Pt.

The 4-electron reduction selectivity of the catalysts for ORR was evaluated using a RRDE. The ORR electron transfer number (n) and hydrogen peroxide yield (H_2O_2 %) were calculated by the following equation, respectively.

$$n = 4 * \frac{i_d * N}{N * i_d + i_r}$$

$$H_2O_2\ \ \% = 200 * \frac{i_r / N}{i_d + i_r / N}$$

where i_r is the ring current, i_d is the disk current, and N stands for the calibrated collective efficiency of the RRDE (N = 0.26).

Finally, the stability of the catalysts was assessed via an accelerated durability test (ADT) for 10000 cycles with a sweep rate of 50 mV/s within potential range of 0.6-1.0 V vs. RHE.

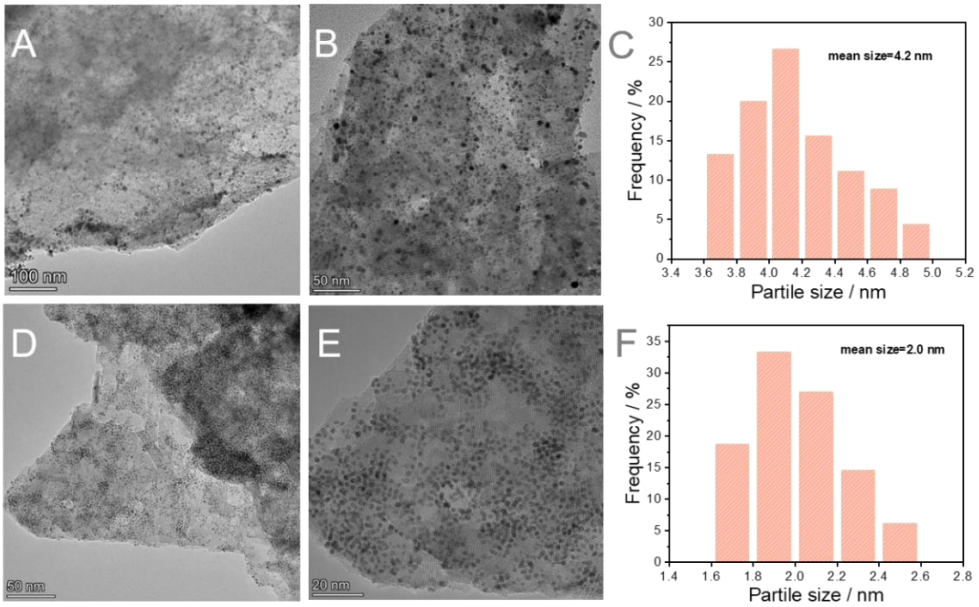

Fig. S1 TEM images and particle size distribution of P-PtNi@N,C-TiO_2 NPs (A-C) and PtNi@N,C-TiO_2 NPs (D-F).

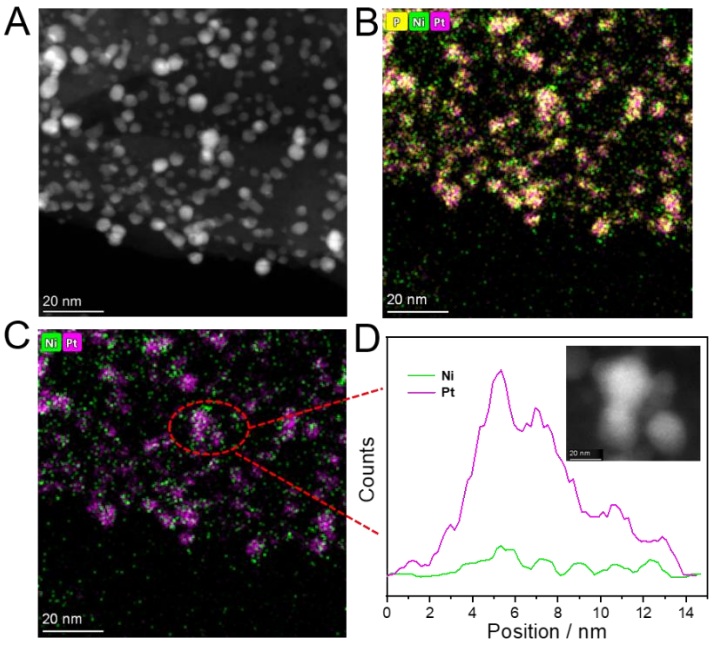

Fig. S2 (A) HAADF-STEM image of P-PtNi@N,C-TiO_2 NPs, (B,C) elemental mapping mixed distribution of P-PtNi@N,C-TiO_2 NPs, (D) EDS line-scanning profile of Pt, Ni elements across P-PtNi@N,C-TiO_2 NPs (scale bars:20 nm).

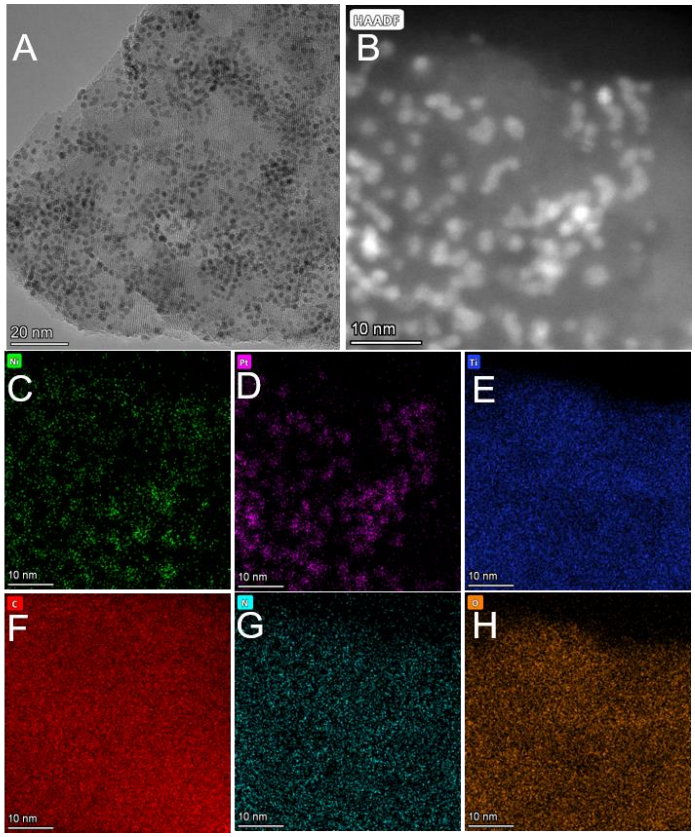

Fig. S3 (A)TEM image (scale bars:20 nm), (B) HAADF-STEM image and (C-H) elemental mapping distribution of PtNi@N,C-TiO_2 NPs (scale bars:10 nm).

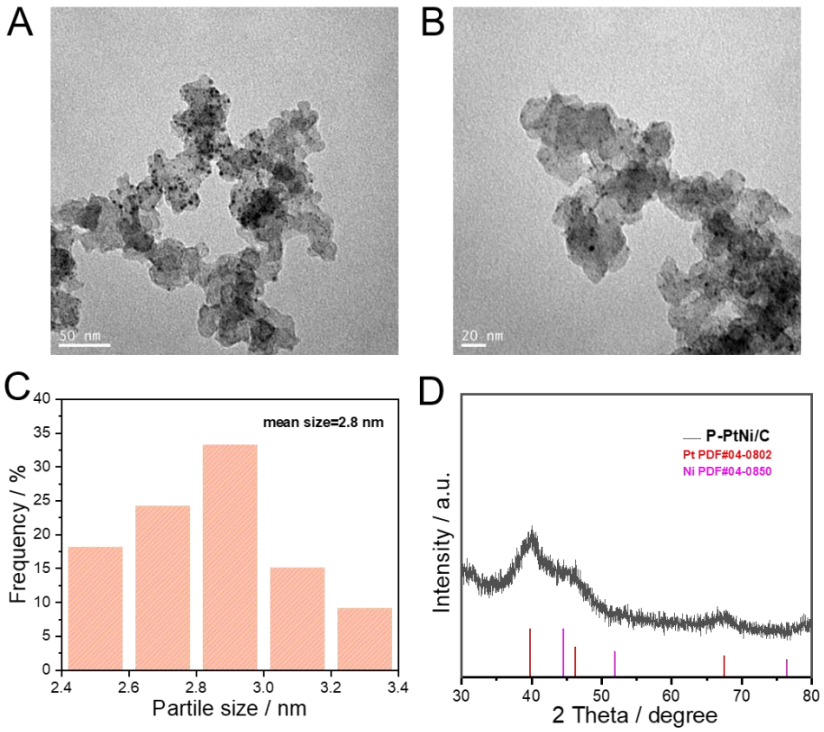

Fig. S4 TEM images (A, B), particle size distribution (C), and XRD pattern of P-PtNi@C (D).

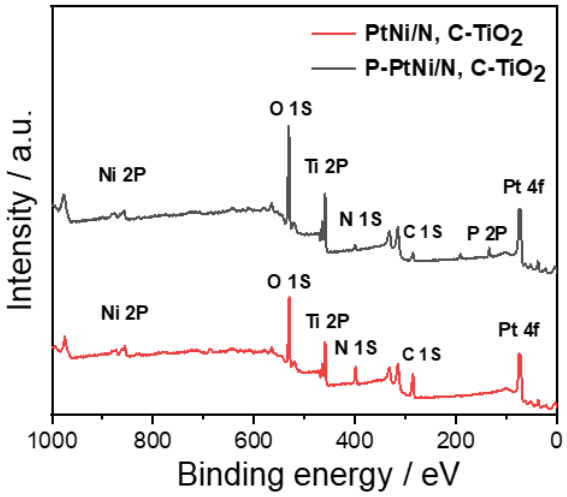

Fig. S5 XPS spectra of P-PtNi@N,C-TiO_2 NPs and PtNi@N,C-TiO_2 NPs.

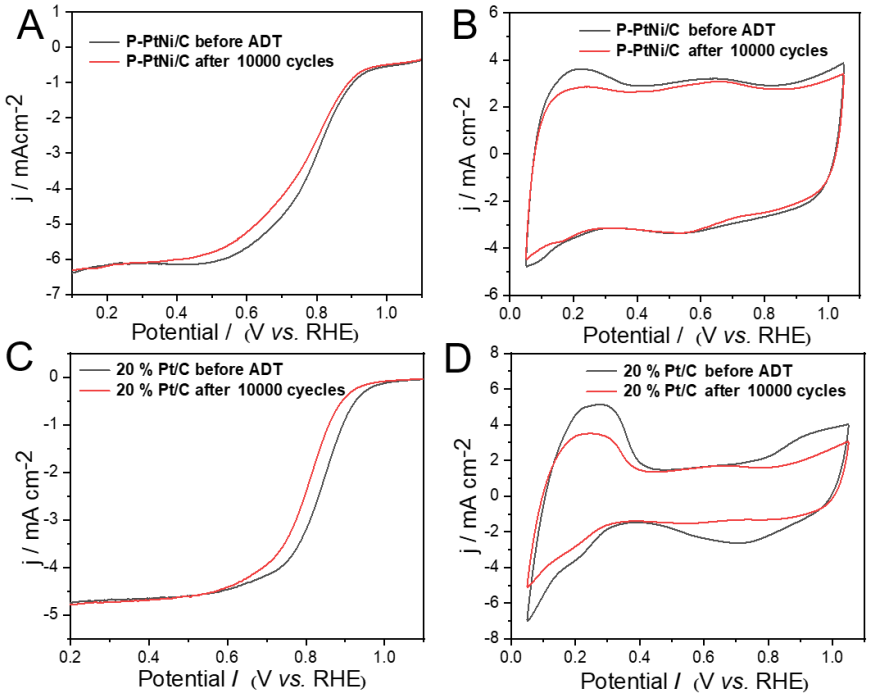

Fig. S6 LSV curves of P-PtNi@C (A) and 20% Pt/C (C) before and after 10 000 potential cycles in potential range of 0.6-1.0 V at 1600 rpm in O_2-saturated 0.1 M $HClO_4$ solution. CV curves of P-PtNi@C (B) and 20% Pt/C (D) before and after ADT in Ar-saturated 0.1 M $HClO_4$ solution.

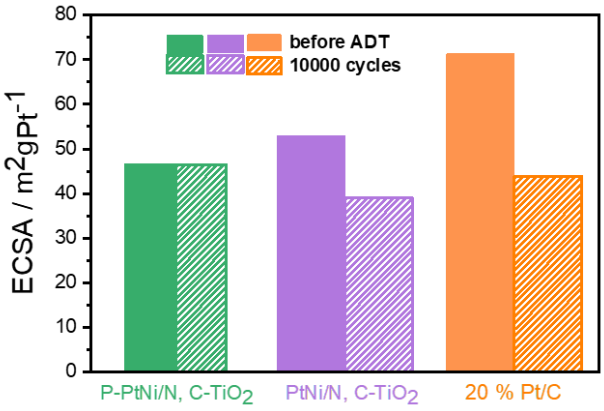

Fig. S7 ECSA of P-PtNi@N,C-TiO_2, PtNi@N,C-TiO_2 and 20% Pt/C before and after ADT in 0.1 M $HClO_4$ solution.

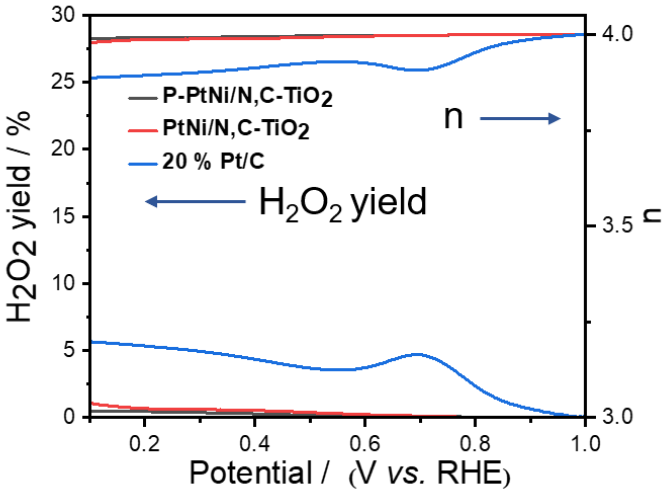

Fig. S8 Electron transfer number (n) and H_2O_2 yield of P-PtNi@N,C-TiO_2, PtNi@N,C-TiO_2 and 20% Pt/C for ORR in 0.1 M $HClO_4$.

Table S1 Elemental contents of P-PtNi@N,C-TiO_2 NPs and PtNi@N,C-TiO_2 NPs measured by XPS.

Catalyst	C	N	O	Ti	Pt	Ni	P
	at %	at %	at %	at %	at %	at %	at %
P-PtNi@N,C-TiO_2	5.41	9.37	49.79	12.49	6.57	13.52	2.85
PtNi@N,C-TiO_2	35.35	14.97	31.72	9.27	5.77	2.92	0

Table S2 Pt, Ni and P element content in P-PtNi@N,C-TiO_2 NPs, PtNi@N,C-TiO_2 NPs and P-PtNi@C NPs measured by ICP-OES.

Catalyst	Pt wt %	Ni wt %	Pt:Ni molar ratio	P wt %
P-PtNi@N,C-TiO_2	9.7	2.64	1.11	3.57
PtNi@N,C-TiO_2	8.28	2.46	1.02	0
P-PtNi@C	6.25	1.84	1.03	1.75

Table S3 Comparison of catalytic performance with previously reported catalysts

Catalyst	The loading of Pt (ug cm^{-2})	Mass activity (A mg_{Pt}^{-1}) @0.9V (vs. RHE)	Specific activity (mA cm^{-2}) @0.9V (vs RHE)	Mass Activity loss, cycles (0.6-1.0V vs RHE)	Reference
P-PtNi@N,C-TiO_2	22	0.53	1.13	10000 cycles 11.3%	This work
20 % Pt/C	100	0.13	0.18	10000 cycles 39 %	This work
Pt-TiO_{2-x} NS	16.8	0.314	0.314	10000 cycles 32 %	4
Pt/$Ti_{0.8}Co_{0.2}O_2$ NTAs	25	0.53	0.96	10000 cycles 8 %	5
WO_x-PtNi NWs	/	0.85	1.29	30000 cycles 23.89 %	6
Pt_3Cu/TiN	10.2	2.43	5.32	10000 cycles 16.1 %	7
Pt/TPY/TNTS-Mo	10	0.12	1.2	10000 cycles 4.2 %	8
Pt/TiO_2-C	20.4	0.205	0.256	10000 cycles 0.9 %	9
PtCo/TiO_2/CNT	80	0.46	0.606	30000 cycles 11.24 %	10

References

1. J. Wan, W. Chen, C. Jia, L. Zheng, J. Dong, X. Zheng, Y. Wang, W. Yan, C. Chen, Q. Peng, D. Wang and Y. Li, *Adv. Mater.*, 2018, **30**, 1705369.
2. J. Guan, S. Yang, T. Liu, Y. Yu, J. Niu, Z. Zhang and F. Wang, *Angew. Chem. Int. Ed.*, 2021, **60**, 21899-21904.
3. S. He, Y. Liu, H. Zhan and L. Guan, *ACS Catal.*, 2021, **11**, 9355-9365.
4. K. M. Naik, E. Higuchi and H. Inoue, *J. Power Sources*, 2020, **455**, 227972.
5. F. Yu, Y. Xie, L. Wang, N. Yang, X. Meng, X. Wang, X. L. Tian and X. Yang, *Electrochim. Acta*, 2018, **265**, 364-371.
6. Y. Mo, S. Feng, T. Yu, J. Chen, G. Qian, L. Luo and S. Yin, *J. Colloid Interface Sci.*, 2022, **607**, 1928-1935.
7. Z. Wu, D. Dang and X. Tian, *ACS Appl. Mater. Interfaces*, 2019, **11**, 9117-9124.
8. R. Alipour Moghadam Esfahani, H. M. Fruehwald, N. O. Laschuk, M. T. Sullivan, J. G. Egan, I. I. Ebralidze, O. V. Zenkina and E. B. Easton, *Appl. Catal., B*, 2020, **263**, 118272.
9. J. Wang, M. Xu, J. Zhao, H. Fang, Q. Huang, W. Xiao, T. Li and D. Wang, *Appl. Catal., B*, 2018, **237**, 228-236.
10. F. Cao, H. Zhang, X. Duan, X. Li, R. Ding, K. Hua, Z. Rui, Y. Wu, M. Yuan, J. Wang, J. Li, M. Han and J. Liu, *ACS Appl. Mater. Interfaces*, 2022, **14**, 51975-51982.